Ceramics International 42 (2016) 17764–17772

Contents lists available at ScienceDirect

Ceramics International

journal homepage: www.elsevier.com/locate/ceramint

Use of polymeric fibers to increase gas permeability of lanthanum carbide based targets for nuclear physics applications

S. Corradetti [a,*], L. Biasetto [a,b], M.D.M. Innocentini [c], S. Carturan [a,d], P. Colombo [e], A. Andrighetto [a]

[a] INFN Laboratori Nazionali di Legnaro, Viale dell'Università 2, Legnaro (PD) 35020, Italy
[b] Università di Padova, Dipartimento di Tecnica e Gestione dei Sistemi Industriali, Stradella S. Nicola 3, Vicenza 36100, Italy
[c] Curso de Engenharia Química, Universidade de Ribeirão Preto, Ribeirão Preto, SP 14096-900, Brazil
[d] Università di Padova, Dipartimento di Fisica e Astronomia, via Marzolo 8, Padova 35131, Italy
[e] Università di Padova, Dipartimento di Ingegneria Industriale, via Marzolo 9, Padova 35131, Italy

ARTICLE INFO

Article history:
Received 14 June 2016
Received in revised form
5 August 2016
Accepted 17 August 2016
Available online 18 August 2016

Keywords:
B. Porosity
B. Fibers
D. Carbides
E. Nuclear applications

ABSTRACT

Porous lanthanum carbide disks were prepared from La_2O_3 and graphite powders and with additions of polymeric fibers as sacrificial templates for the formation of interconnected channels of enhanced permeability to gas flow. Two kind of fibers were used (Nylon 6,6 and polypropylene) characterized by an average length of 500 μm and diameters of 18 and 20 μm, respectively. The fiber content was varied up to 21.3 vol% for nylon or up to 24.8 vol% for PP in order to control the porosity and the permeability level of bodies. The fiber-derived porous LaC_x samples exhibited higher total porosity (38.0–51.7% for PP and 42.9–55.3% for nylon) compared to standard LaC_x where porosity (35.7%) was generated only by the carbothermal reaction during sintering. A 50-fold increase in the Darcian permeability coefficient k_1 and a 1200-fold increase in the non-Darcian coefficient k_2 were achieved in comparison with the permeability level of the composition without fibers ($k_1 = 1.21 \times 10^{-15}$ m^2 and $k_2 = 1.17 \times 10^{-11}$ m). Nylon was slightly better than PP to enhance permeability of LaC_x targets.

1. Introduction

In the last years much effort has been devoted to the improvement of the release efficiency of short-lived isotopic species (Radioactive Ion Beams, RIBs) in Isotope Separation On-Line facilities (ISOL), with particular reference to the characteristics of the target material [1–5].

The primary factors that govern the intensity of RIBs at ISOL based research facilities include: a) the energy, atomic number and intensity of the primary beam; b) the cross-section for production of the radioactive ion species; c) the lifetime of the species of interest; d) the dimension, density and geometry of the target materials; e) the maximum temperature at which targets can be operated; f) the dimensions, geometry and materials of construction of the vapor transport system and g) the ionization efficiency of ion sources chosen for RIB generation.

Diffusion and effusion represent the two main mechanisms for isotopes to escape from the target. Diffusion can be thermally and/or radiation enhanced [6]: isotopes migrate from the crystal lattice to the grain boundaries and their diffusion is governed by Fick's laws. From the grain boundaries, the isotopes must then effuse through the empty spaces of the target according to a molecular flow governed by the mean number of collisions with the target material and the internal walls of the box containing the target, the mean sticking time per collision and the mean flight time between collisions [7]. The target unit must therefore operate under high vacuum and at the highest temperature possible, taking into account the thermal properties of the material constituting the target and the target envelope.

Within the SPES project, now under construction at Laboratori Nazionali di Legnaro, Italy [8], this research group is currently studying the gas permeability properties of different porous targets based on LaC_2 or LaOC. Lanthanum is chosen as substitute material for uranium, owing to its similar chemical and physical properties.

Recently, LaC_2-LaOC-C foams were developed using polymethylmetacrylate (PMMA) micro-beads as sacrificial filler and phenolic resin as source of carbon and binder. Gas permeability measurements were performed both at room temperature and at 450 °C under argon flow. Gas permeability data revealed that it was possible to tailor the amount of open porosity by varying the amount of PMMA micro-beads and that gas permeability

* Corresponding author.
E-mail address: stefano.corradetti@lnl.infn.it (S. Corradetti).

http://dx.doi.org/10.1016/j.ceramint.2016.08.104
0272-8842/

measurements represented an efficient tool for process control [9].

For permeation purposes, there are many advantages in using fibers as sacrificial fillers [10–13] over powders and micro-beads: a) fibers are elongated in shape and yield a much higher "path length to filler content" ratio, thereby enabling to span over longer distances inside the matrix for the same mass of sacrificial filler; b) channels created by fibers are less tortuous and with smoother walls, thus reducing the fluid dynamic drag and increasing permeability; c) due to their elongated shape, fibers have higher probability to intercept each other, creating a net of interconnected paths throughout the matrix.

The literature contains plenty of examples in which fibers, or combinations of fibers and micro-beads, are used as sacrificial fillers to enhance the permeability of ceramic matrices. Polypropylene fibers in particular have been extensively used to improve the permeation features of dense matrices [14–18].

In the case of the LaC_x or UC_x targets in the SPES project, although not driven by a pressure gradient, the release of exotic species is more effective if a net of interconnected voids is available to minimize the release time from the target before the particle decay. In this case, permeability is an indirect measurement of how efficient are the connections between the bulk and the surface of the target [9].

In the present work, polymeric fibers were used as pore formers for the production of lanthanum carbide targets with enhanced permeability. The main goal was the development of interconnected channels capable of improving the permeability constants of the produced materials, while maintaining a high enough mechanical integrity to allow handling and characterization.

The effect of fibers composition, geometric characteristics and volume percentage on the morphology of the produced LaC_x porous structures was investigated.

2. Material and methods

La_2O_3 powder, graphite powder (both from *Sigma-Aldrich*), phenolic resin powder (*Dynea, 860 series*) and polymeric fibers (*Flinco Fibras Ltda, Brazil*) were used as starting materials for the synthesis of LaC_2-based porous materials. La_2O_3 and graphite powder acted as La and C sources, respectively, according to the reaction (which in high vacuum starts above 1000 °C [3]):

$$La_2O_3 + 11C \rightarrow 2LaC_2 + 4C + 3CO \quad (1)$$

A first batch (blank) was prepared without fibers, representing the prototype of the standard material for the SPES target. In the next batches, different volumes of polymeric fibers of two different materials (nylon 6,6 and polypropylene) of same length (500 μm) and similar diameters (18 and 20 μm, respectively) were added to promote, by their burnout, the creation of a network of oriented interconnected and permeable pores. Phenolic resin was used as a binder (2% based on the weight of the La_2O_3+C+resin mixture).

The mixing of the powders and fibers was performed in two different stages, in a planetary ball mill (*Retsch PM 100, Retsch, Germany*) with agate spheres (diameter of 10 mm) and a 250 mL jar. In the first stage, only La_2O_3, graphite and the resin were mixed, at medium rotation speed (400 rpm) with a balls-to-powder mass ratio of about 6:1. The second stage of mixing involved the polymeric fibers, which were added to the previously obtained reagents mix. In this case, a 2:1 balls-to-powder ratio was used, at a rotation speed of 150 rpm. The choice of this particular mixing configuration was driven by the need of preserving the fibers shape and integrity during the mixing, thereby promoting the creation of straight channels into the final material.

The mixed powders were shaped in form of disks by means of uniaxial cold pressing at 750 MPa inside a specifically manufactured die with an internal diameter of 40 mm. The disks containing fibers underwent two sequential thermal treatments. The first one was from room temperature to 1000 °C, with a heating rate of 2 °C/min in argon atmosphere (tube furnace) and a dwell time of 6 h, followed by cooling down at ~2 °C/min (approximate value due to thermal inertia, especially for temperatures close to RT). The purpose of this treatment was to decompose the fibers and the phenolic resin, which leaves a carbon residue of about 45 wt% [19], and to achieve complete release of moisture and CO_2 (~3% total weight loss) from La_2O_3.

The second thermal treatment was up to 1750 °C (no dwell time), with a heating rate of 2 °C/min and intermediate steps of 6 h at 1200 °C, 1400 °C and 1600 °C followed by cooling down at ~2 °C/min. This treatment was performed in a high vacuum furnace specifically designed for LaC_2 [20], with the aim of allowing Reaction (1) to occur and to sinter the formed LaC_2 grains around the created channels. In the case of the blank samples, only the second treatment was carried out, with no preliminary burnout stage.

Differential thermal (DTA) and thermogravimetric analyses (TGA) were performed on the raw fibers and La_2O_3 powders with a heating rate of 10 °C/min in argon (*STA 410, Netzsch-Gerätebau GmbH, Germany*).

The volumetric fraction of fibers (f_v) in each green sample was calculated by:

$$f_v = \frac{f_m \rho_{green}}{\rho_{fiber}} \quad (2)$$

in which f_m is the added fiber mass fraction, ρ_{green} is the experimental green bulk density of the disk after pressing (g/cm^3) and ρ_{fiber} is the fiber solid density (1.14 g/cm^3 for nylon and 0.91 g/cm^3 for PP).

The bulk density (ρ_{bulk}) of the sintered samples was calculated by the mass over volume ratio, while the theoretical density (ρ_{th}) of the final composition (LaC_2+2C) was obtained using the expression:

$$\rho_{th} = f_{LaC_2}\rho_{LaC_2} + f_C\rho_C \quad (3)$$

in which f_{LaC2} and f_C are the volumetric fractions of LaC_2 and free carbon present in the sintered sample, respectively, and ρ_{LaC2} and ρ_C are the theoretical solid densities of the two components (5.02 g/cm^3 for LaC_2 and 1.90 g/cm^3 for graphite) [2]. The presence of LaC_2 and C only, as a result of this type of thermal treatment, was previously reported in [2].

Total porosity (ε_{total}) was calculated by:

$$\varepsilon_{total} = 1 - \frac{\rho_{bulk}}{\rho_{th}} \quad (4)$$

The microstructure of the raw fibers and green and sintered samples was observed by Scanning Electron Microscopy (*SEM, Vega 3xmh, Tescan*), in order to verify the fibers quality before and after milling/pressing and the formation of straight channels and their orientation with respect to the disks geometry after the thermal treatment.

Based on the IUPAC terminology [21], the presence of micro (< 2 nm) and meso (< 50 nm) pores was analyzed by nitrogen physisorption (*ASAP 2020, Micromeritics Italia*). The nitrogen adsorption/desorption isotherms were collected for relative pressures (P/P_{sat}) ranging from 10^{-4} up to 1.0, where P_{sat} is the saturation pressure of nitrogen at the analysis temperature (77 K). The BET method (Brunauer, Emmett, Teller) [22] was applied in

the range of relative pressure between 0.05 and 0.30 for the derivation of the specific surface area of the samples.

Permeability measurements were performed on at least two specimens for each composition, with argon flow at room temperature (T=21–23 °C) and atmospheric pressure (P_{atm}=101.2 kPa). The setup was entirely manufactured at INFN-LNL, following previously reported experimental apparatuses [13]. The test specimen (diameter of =4.0 cm and =1.7–1.8 cm thick) was sealed with annular rubber rings within a cylindrical aluminum sample holder that provided an useful medium diameter of 1.40 cm and a flow area (A_{flow}) of 1.54 cm^2. The argon volumetric flow rate (Q) was measured by a glass-made soap-bubble flowmeter (0.1–4.2 L/min) at the exit of the sample holder and converted to superficial velocity (v_s) by $v_s=Q/A_{flow}$. The pressure drop across the specimen (ΔP) was measured by a digital micro-manometer (0–2000 Pa, *GMH 3161-13 CE, Greisinger electronic GmbH, Germany*). For a reliable fitting analysis, at least 10 sets of flow rate and pressure drop data were acquired, controlling Q by a needle valve and reading the correspondent ΔP value.

The experimental dataset was used to fit permeability coefficients according to Forchheimer's equation for flat media under compressible flow [9,18,23]:

$$\frac{P_i^2 - P_o^2}{2P_oL} = \frac{\mu}{k_1}v_s + \frac{\rho}{k_2}v_s^2 \quad (5)$$

in which P_i and P_o are respectively the inlet and outlet absolute gas pressures ($P_i = P_o + \Delta P$ and $P_o = P_{atm}$), v_s is the superficial gas velocity, L is the medium thickness along the flow direction (measured for each sample), μ is the argon viscosity ($\approx 2.2 \times 10^{-5}$ Pa s) and ρ is the argon density (≈ 1.66 kg/m^3) calculated for outlet flow conditions. The parameters k_1 and k_2 are respectively known as the Darcian and non-Darcian permeability coefficients, in reference to Darcy's law [9,23].

3. Results and discussion

The initial appearance of the nylon and PP fibers tested in this work is shown in the SEM images of Fig. 1a–b. The PP fibers appear to be more packed into bundles compared to the nylon ones. The image of PP fibers incorporated into the green mixture is shown in Fig. 1c, proving that the mild ball mixing conditions applied (low balls to powder ratio and low rotation speed) allowed to preserve the overall morphology of fibers. As a matter of fact, it was observed during preliminary optimization tests that, using higher rotation speed and balls to powder ratio, the fibers were flattened and cracked. The reduction of only one of the two parameters was not sufficient to maintain the fibers integrity during the mixing stage. It is worth noting that the adopted mixing conditions enabled to efficiently loosen the fiber bundles and homogeneously

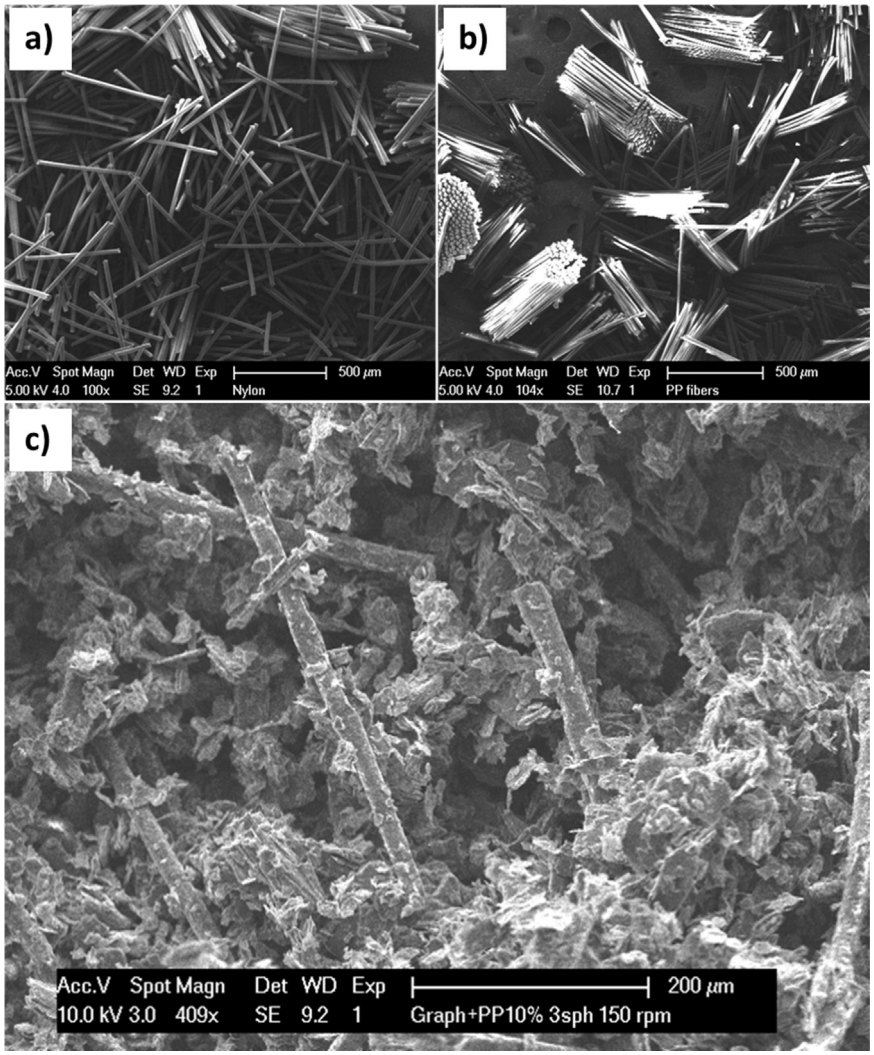

Fig. 1. SEM images of fibers: a) nylon; b) PP; c) PP fibers incorporated into the green composition after low-speed ball mixing.

disperse the PP fibers within the matrix. Also in the case of nylon fibers, which showed less problems than PP in terms of dispersion and integrity, the above described mixing conditions proved to be efficient.

The TGA and DTA curves under argon flow for *as received* nylon and PP fibers and for lanthanum oxide (La_2O_3) are shown in Fig. 2. For both types of fibers, the degradation follows typical profiles given in literature [24,25]. In the case of nylon an additional portion of weight loss was observed at about 100 °C, due to the release of adsorbed water; nylon is well known for its tendency to adsorb water due to the presence of polar and hydrogen bonding amide groups. La_2O_3 weight loss includes water, CO and CO_2 releases, which are completed at 800 °C [3].

The comparison between the theoretical and observed weight losses is shown in Fig. 3. The theoretical weight loss takes into consideration the CO release during the occurrence of the Reaction (1), as well as the weight losses of phenolic resin, fibers and lanthanum oxide, as reported in the TGA-DTA analysis in Fig. 2.

The observed weight losses fairly agree with the theoretical values, being in general a little higher. The differences can be attributed to: a) loss of material during the transport and handling of material; b) changes in the humidity absorption of raw materials throughout the samples preparation campaign; c) local uncontrolled variations of the thermal treatments parameters

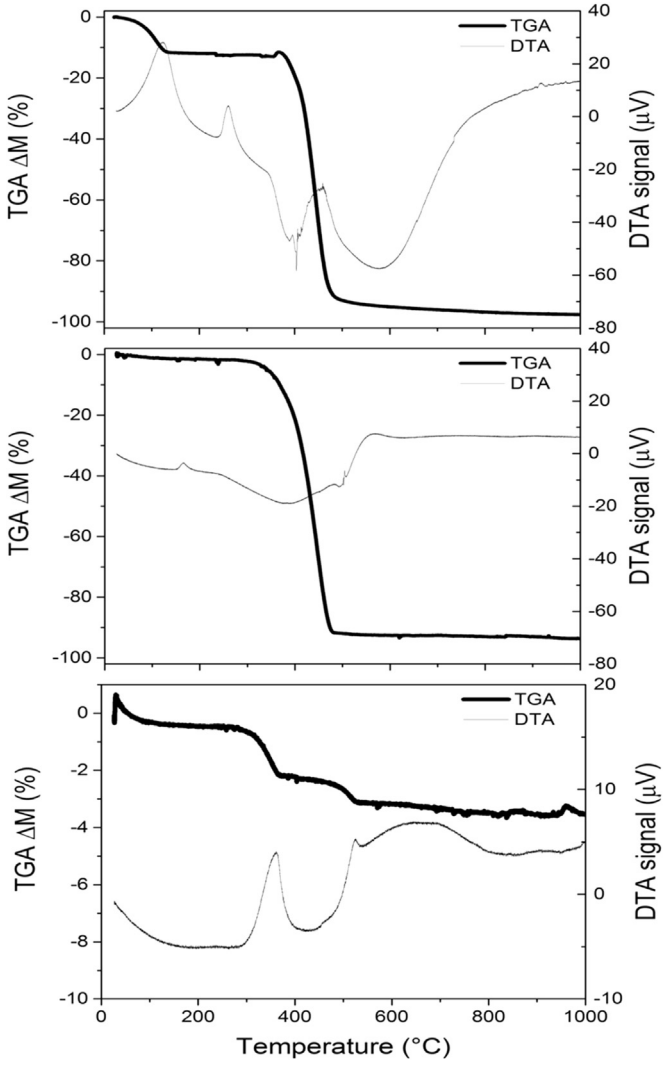

Fig. 2. TGA/DTA under argon flow and heating rate of 10 °C/min for raw materials: (a) nylon fiber; b) polypropylene fiber; c) Lanthanum oxide.

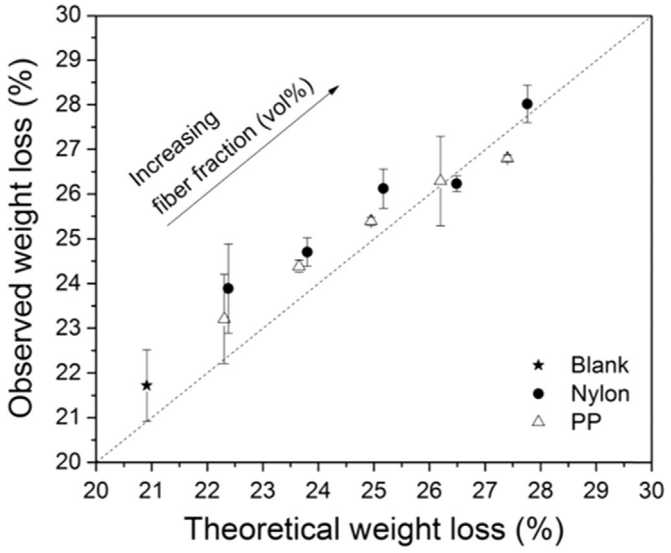

Fig. 3. Comparison between the theoretical and observed weight losses for samples with different types and fraction of fibers.

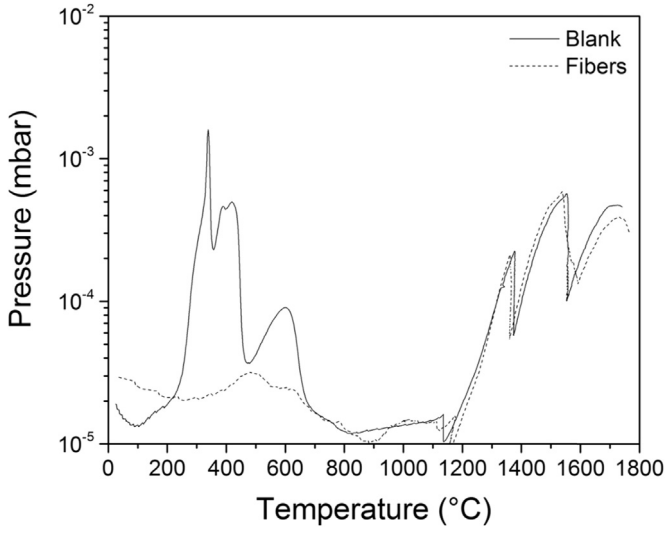

Fig. 4. Vacuum evolution in the reaction chamber during the second thermal treatment of samples with or without (blank) fibers.

(vacuum, temperature, gas flow) which could have had an effect on the production process, especially on the progress of Reaction (1).

The gas evolution during the second thermal treatment of samples is shown in Fig. 4, where the absolute pressure inside the reaction chamber is reported for blank and fiber containing samples (only one is reported as an example). Some differences are clear between the curves. Four peaks in the 200–1000 °C range can be observed for the blank sample, which are associated with the release of H_2O and CO_2 during the decomposition of the phenolic resin [26]. This behavior was not observed in the treatment of the samples obtained using fibers, since in those cases the decomposition of the binder was achieved during the first thermal treatment, along with the burnout of the fibers. A smaller amount of gas was however released from the samples with fibers, corresponding to the residual decomposition of previously unburned species. In both samples a similar gas evolution can be observed above 1000 °C, due to the release of CO according to Reaction (1), which was temporarily interrupted during the 6-hour intermediate stops at 1150 °C, 1375 °C and 1550 °C. This behavior was

confirmed by previous studies [3]. These steps were slightly different from those expected (1200 °C, 1400 °C and 1600 °C, as of Fig. 2) due to local deviations of the heating system with respect to the furnace calibration, but were considered similar enough to the desired temperatures. The fact that samples with and without fibers had the same behavior, in terms of carbothermal reaction, confirms the efficiency of the mixing procedure between La_2O_3 and graphite powders also in the presence of fibers.

As observed in the SEM images shown in Figs. 5 and 6, the increase in the fiber fraction clearly resulted in the creation of an increasing number of straight channels in the internal sections of the sintered bodies. The created channels are radially (parallel) oriented to the disks faces due to the uniaxial pressing conditions. If not accompanied by the creation of a sufficient number of interconnections, these channels could not be translated into the most efficient enhancement of fluid flow, which occurs when channels are oriented along the axial direction connecting the disk faces. This aspect has been investigated by several works whose intent was the increase of permeability in ceramic structures for different applications. Isobe et al. [27,28] produced porous alumina bodies of aligned porosity using nylon fibers (up to 30 vol% with average diameters of 9.5–43 μm and length of 800 μm) or carbon fibers (52 vol% with average diameter of 14 μm and length of 600 μm). In their case, fibers were aligned in the matrix along the flow direction by an extrusion method. Despite the different orientation, the channel morphology observed by SEM was very similar to those presented in Figs. 5–6. The same channel morphology was observed in extruded bodies produced by Okada et al. [10,29,30] who added up to 20 wt% rayon or polylactic acid (PLA) fibers with 12–29 μm in diameter and 500–800 μm in length in alumina, mullite and metakaolin-based matrices and by Rasouli et al. [11], who reported additions up to 40 vol% of PLA fibers of 12–29 μm in diameter and 500 μm in length in metakaolin-based geopolymers shaped by a hand-extruder. Polymeric fibers have also been added in refractory castables to reduce the risk of explosive spalling during the drying-sintering stages [12–17] and in molds for investment casting to help the fast release of gases during the mold filling with liquid metals [18,31]. The preferred fibers in these applications are nylon and PP, with 0.1–24 mm in length and 15–20 μm in diameter, but with content usually below 1 vol% in order to avoid substantial decrease in mechanical strength. The usual molding method is the casting of slurries, which provides a non-oriented dispersion of fibers in the ceramic matrices. In the case of refractory castables, the presence of coarse aggregates in the matrix has led to aggressive mixing conditions of the ceramic slurry or paste and the damage of fibers, with generation of irregular channels and partial loss of the benefit in permeability. Interesting details of the porous microstructure and discussion of mechanisms for permeability increase of fiber-based castables and molds for investment casting are reported by Innocentini et al. [12–14,16–18], Salomão and Pandolfelli [32], Salomão et al. [15,33], Mandecka-Kamień et al. [14], Yuan and Jones [31] and Collignon et al. [34].

The beneficial effect of the increase in the fiber fraction on the permeation behavior of sintered samples appears clearly in the normalized pressure drop curves plotted in Fig. 7. The pressure drop level was considerably lowered at the same gas velocity as the fiber fraction increased. This common trend was observed for both nylon and PP fibers. Despite the apparently linearity, Eq. (5) was very well fitted to experimental data ($R^2 > 0.99$), which implies the validity of Forchheimer's equation and the importance of accounting for both the viscous (linear) and inertial (quadratic) terms in velocity to compute the total pressure drop.

The resulting permeability coefficients k_1 and k_2 fitted from

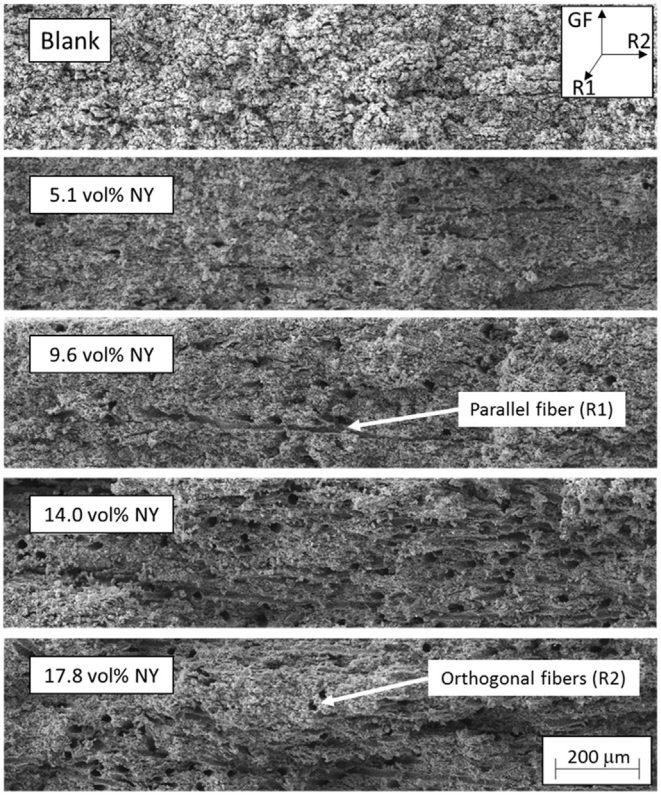

Fig. 5. SEM images of the microstructure of sintered samples prepared with different contents of nylon fibers. GF indicates the gas flow direction during the permeability measurement (along the thickness of the sample), R1 and R2 the radial directions (along the diameter).

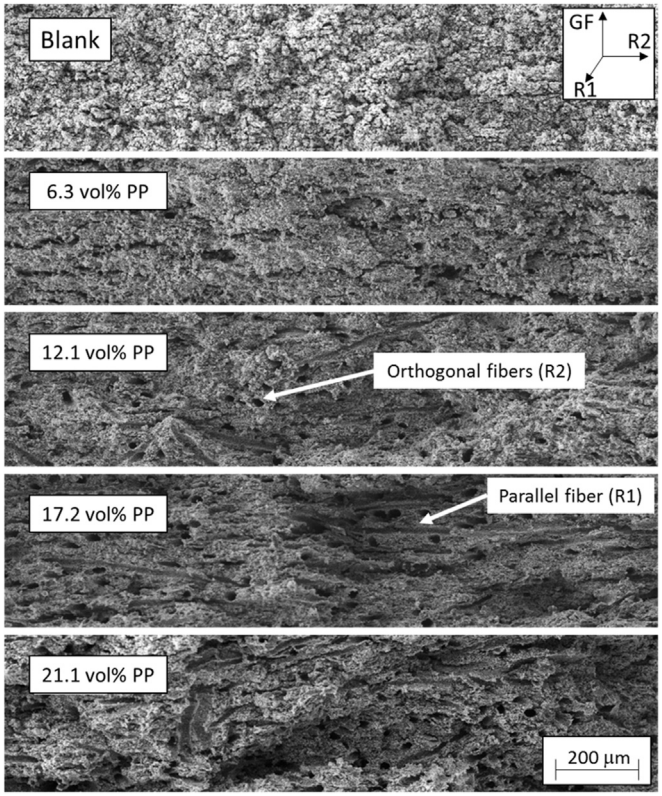

Fig. 6. SEM images of the microstructure of sintered samples prepared with different contents of PP fibers. GF indicates the gas flow direction during the permeability measurement (along the thickness of the sample), R1 and R2 the radial directions (along the diameter).

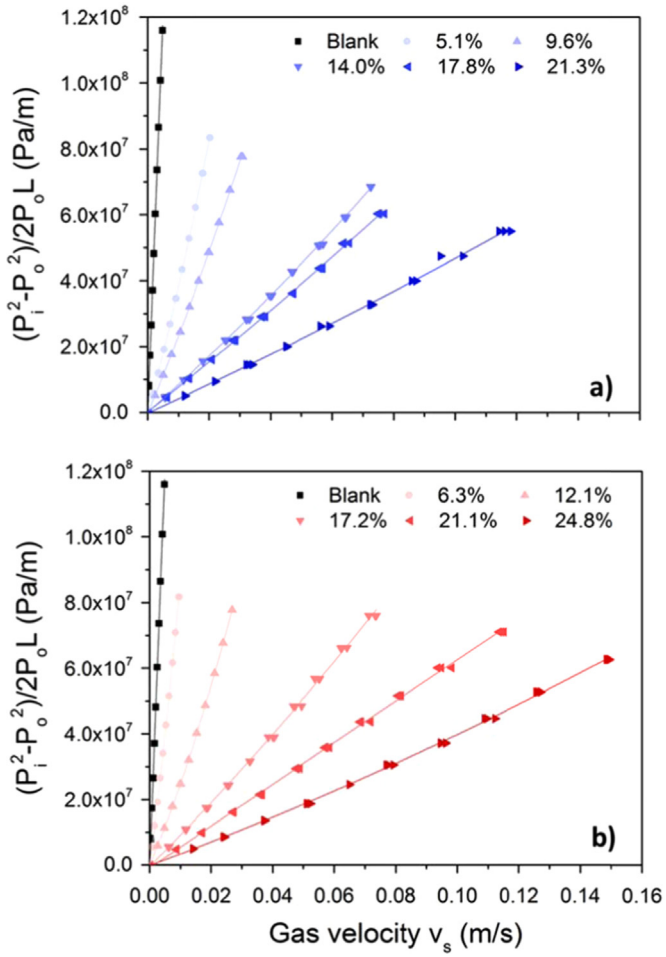

Fig. 7. Experimental permeation curves of sintered samples with different types and volume fractions of fibers: a) nylon; b) PP. Lines are parabolic fittings according to Eq. (5). (Color online).

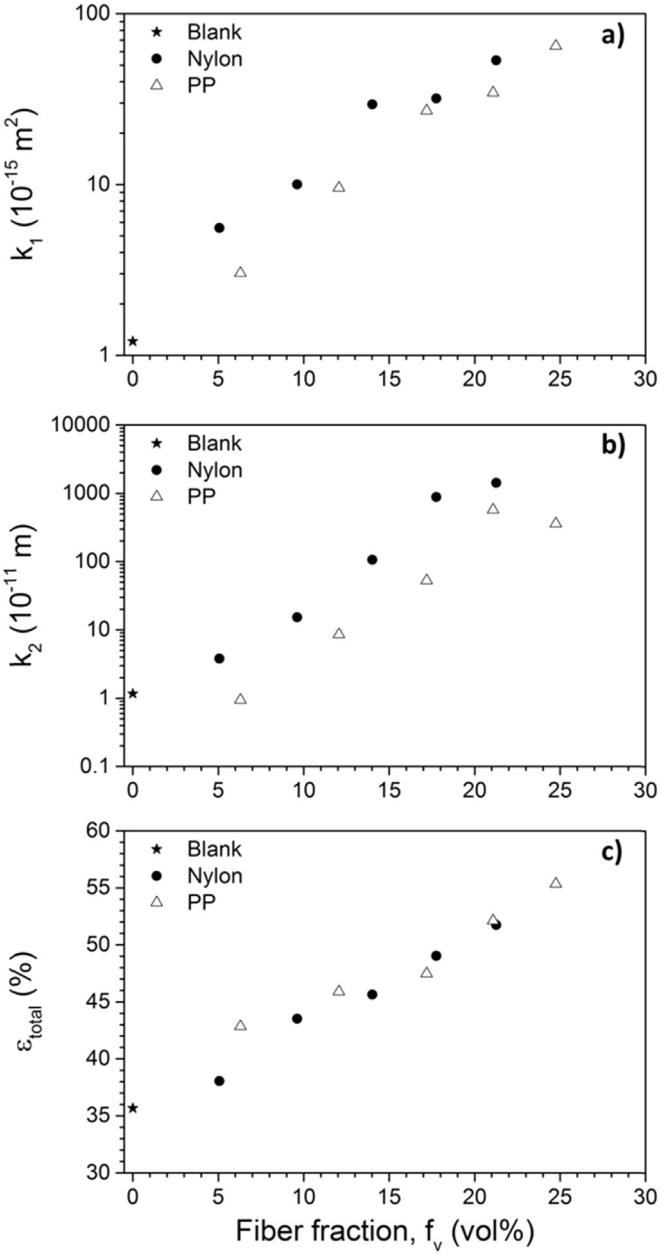

Fig. 8. Influence of type and fraction of fibers on: (a) Darcian permeability coefficient, k_1; (b) Non-Darcian permeability coefficient, k_2; (c) Total porosity, ε_{total}.

curves in Fig. 7 and Eq. (5) are given in Figs. 8a and 8b as a function of the volumetric fiber fraction, f_v. To help analysis, total porosity of samples is also plotted in Fig. 8c.

As expected, the total porosity of bodies followed an almost linear and univocal dependence with the volumetric content of fibers f_v, regardless the fiber type. An addition of ≈ 25 vol% of fibers caused nearly the same increase in total porosity. On the other hand, increases of almost two orders of magnitude for k_1 ($1.21–64.83 \times 10^{-15}$ m^2) and three orders of magnitude for k_2 ($1.17–1426.83 \times 10^{-11}$ m) were achieved with respect to the blank sample. Compared under the same volumetric fiber content, nylon-based samples were slightly more permeable than PP samples, a difference that could not be ascribed to the porosity level. Since both *as received* fibers had nearly similar shapes and dimensions, then it is possible that nylon was more resistant than PP to deformation, abrasion or rupture during processing and therefore was able to create a smoother or more disperse and interconnected network of voids in the ceramic matrix. The better mechanical performance of nylon over PP fibers is already described in the literature on fiber-reinforced concretes [35].

A previous study included PMMA spherical beads as sacrificial fillers to increase the permeability of lanthanum oxycarbide disks [13] used as targets in the SPES project. In that case, a PMMA content of 60.6 vol% was required to raise k_1 and k_2 respectively to 9.43×10^{-14} m^2 and 8.97×10^{-9} m. In the present work, a similar permeability level ($k_1 = 6.48 \times 10^{-14}$ m^2 and $k_2 = 3.6 \times 10^{-9}$ m) was achieved with inclusion of only 24.8 vol% of PP fibers. A similar comparison has been reported by Isobe et al. [27], who added up to 30 vol% of nylon fibers (800 μm long) or up to 50 vol% of PMMA beads (10 μm spheres) in alumina/mullite matrices. Although the porosity increase was nearly proportional to the volume of each filler added, the permeability increase was exponential and much more pronounced in the fiber-containing specimens. It is worth noting that, different from the gelcasting of foams, were air bubbles are merged in several grades to create cells connected through multidirectional windows (throats), the inclusion of solid fillers such as PMMA can only create throats by the direct contact of adjacent spheres, which limits the size of effective flow paths [36]. In such situation, a very large content or a wide size distribution of beads is necessary to ensure cell connectivity and permeability increase.

A survey of permeability data concerning the use of fibers as pore formers in ceramic matrices is presented in Table 1. Extrusion is the preferred molding method of flat filtering membranes, as

Table 1
Comparison of permeability data of fiber-based ceramics reported in the literature with values experimentally found in this work.

Reference	Molding method	Ceramic matrix	Fiber features					k_1 (m^2)
			Type	Length (mm)	Diameter (μm)	Max. content (vol%)	Orientation to flow direction	
[27]	extrusion	alumina	nylon	0.8	9.5–43	30	parallel	$4.1–39 \times 10^{-14}$
[10]	extrusion	mullite	rayon	0.8	16.5	20	parallel	$4.1–5.6 \times 10^{-14}$
[11]	extrusion	metakaolin-based geopolymer	PLA	0.5	12–29	40	parallel	$0.2–1.7 \times 10^{-14}$
[14]	casting	alumina refractory concrete	PP	6–10	16	0.1	non-oriented	$8.2–42.5 \times 10^{-12}$
[34]	casting	alumina refractory concrete	PP	6	50	0.2	non-oriented	$3–300 \times 10^{-17}$
[31]	casting	SiO_2-Al_2O_3-ZrO_2 investments	PP	1	20	20[a]	non-oriented	$5.4–5.8 \times 10^{-7}$
[18]	casting	spinel-based investments	PP	1	20	0.85[b]	non-oriented	$0.8–1.5 \times 10^{-14}$
[12]	casting	alumina refractory concrete	PP, PET, jute, cellulose, nomex	2–6	15–30	0.36	non-oriented	$4–22 \times 10^{-16}$
[15]	casting	alumina refractory concrete	PP	0.1–24	15	0.36	non-oriented	$4–28 \times 10^{-16}$
This work	*uniaxial pressing*	*lanthanum carbide*	*PP and nylon*	*0.5*	*18–20*	*24.8*	*perpendicular*	$1.2–65 \times 10^{-15}$

[a] g/L suspension;
[b] wt%.

pores are aligned in parallel to the flow direction. The fiber content is relatively high (up to 40 vol%) to yield bodies with permeability level around 10^{-14}–10^{-13} m^2. On the other hand, casting of slurries is used for molding of refractory concretes and investments where fibers are randomly dispersed in the ceramic structure. Fiber content in this case is much lower (< 1 vol%), but the permeability increase is also very pronounced when compared to the values of blank samples (10^{-17}–10^{-14} m^2).

Despite the very different fiber contents, the similar effect on permeability in extruded and cast samples is related to the different mechanisms by which fibers act in promoting the creation of flow paths. In concrete materials, the porous structure can be considered a two-phase composite consisting of a matrix paste surrounding a cluster of coarse aggregate grains. The main source of permeable paths is not the porosity of the matrix, but the transition zone formed by wall effects at the matrix–aggregate interface [37]. In this case, fibers are mostly used to link the interfacial zones, which explains the need of much smaller amounts to yield a substantial increase in permeability. The length of fibers is more important than the amount added [15,16,32,33]. On the other hand, in ceramic matrices formed by homogeneous pastes of fine powder mixtures, the interconnected porosity available for fluid flow is randomly distributed throughout the structure and is mostly composed of small pores of irregular shape originated from packing constraints and removal of mixing liquids or volatile compounds. Cracks caused by sintering phenomena also lead to some path creation, although they are in fact deleterious for the mechanical strength and thus avoided as a primary permeability enhancer method. In this situation, fiber channels are not expected to link permeable zones, but to create instead a completely new network for fluid flow. Therefore, the permeability increase is more effective if the channels created by the fibers burnout are axially aligned to the fluid flow direction linking the opposite surfaces exposed to the fluid pressure gradient. Other fiber orientations may also be effective, as long as a net of interconnected channels is formed throughout the structure. In either case, a large amount of fibers is required, as observed in the works listed in Table 1. Considering the volume of each PP fiber (500 μm long and 20 μm thick) as $\approx 1.6 \times 10^{-7}$ cm^3, the addition of 1 vol% PP will result in the creation of ≈64,000 channels with total length of

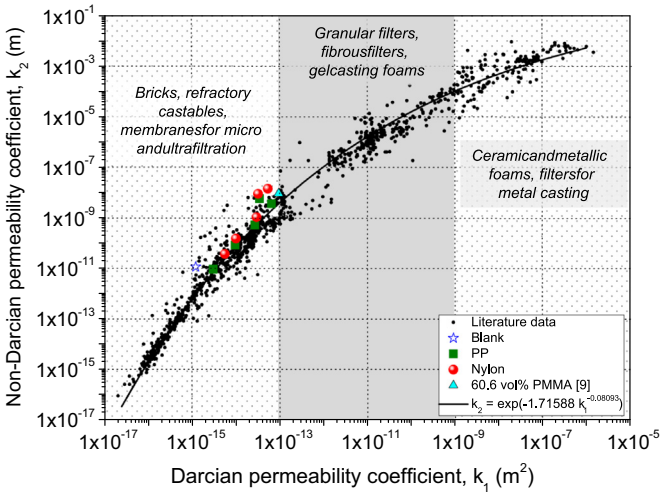

Fig. 9. Permeability map with classification of porous materials and location of blank and fiber-containing LaC_2 samples. Adapted from Biasetto et al. [9].

32 m per cm^3 of sample. These figures increase to ≈1,600,000 channels and ≈800 m per cm^3 for a 25 vol% PP content, and very similar results are obtained with nylon fibers, with density and dimensions slightly different from those of PP. These expressive numbers indicate that some degree of interconnection linking both samples surfaces is expected, even with the molding method (uniaxial pressing) favoring the radial channel alignment. This would justify the permeability increase observed in Fig. 8.

As a basis of comparison with other porous structures, the permeability coefficients k_1 and k_2 are plotted in Fig. 9 in a comprehensive permeability map proposed by Innocentini et al. that includes a large number of data for different types of porous materials [9,18,23]. The location of data from this study suggests that both fiber types yielded permeability levels that belong typically to low permeability concretes, castables and bricks, especially in the case of the blank sample. On the other hand, the samples prepared using higher volumetric fractions of fibers were found to have permeability coefficients similar to those of foams produced by gelcasting or granular and fibrous filtering media.

The shape of the nitrogen physisorption isotherms for selected samples are shown in Fig. 10. The blank sample, produced without using fibers, and nylon- and PP-based samples produced with the maximum fibers loading display quite similar adsorption-desorption isotherms. The main features are the absence of micropores, as proved by negligible adsorption in the low pressure region, the presence of a small hysteresis in the high pressure region, between 0.6 and 0.9, and the steep increase in adsorption up to the saturation pressure. The unambiguous assignment of the isotherm to a specific IUPAC category is not straightforward, being the shape intermediate between type III and type V [21]. Irrespectively of the isotherm type, the samples are macroporous in nature, as demonstrated by the non saturation of the adsorption branch at high pressures. Moreover, the shape of the hysteresis loop, which can be ascribed to a H3 type according to the IUPAC classification [21], points to the presence of a wide and irregular distribution of mesopores (< 50 nm). The differences in specific surface area (SSA) between the blank and the two types of samples, either nylon or PP fibers containing, are almost negligible, being 2.7 m^2/g the SSA value for the blank sample and around 2.6 (nylon) and 3.5 (PP) m^2/g for the samples with the highest fibers loading. SSA is indeed a parameter that is subject to remarkable variations in the case of micro-mesoporous structures, which is not the case for the samples here reported. It is however important to take into account this property in the case of targets for isotopes production, since the presence of interconnected small pores uniformly distributed in the material proved to have a positive effect on the release of isotopes [1,38]. It should be observed that the SSA trends are not in conflict with the permeability data, which are correlated mainly to the presence of the macropores generated by the decomposition of the fibers. O'Brien et al. [39] obtained an inverse correlation between fluid permeability and SSA in collagen scaffolds for tissue engineering, motivated by the presence of frictional effects of fluid flow by the scaffold struts. For the materials considered in the present work however it is clear that an eventual increase in SSA, obtained by the presence of micro-meso pores formed during the fibers decomposition process, would have a negligible effect on permeability due to the presence of a large amount of straight, preferential macrochannels which allow an unhampered fluid flow.

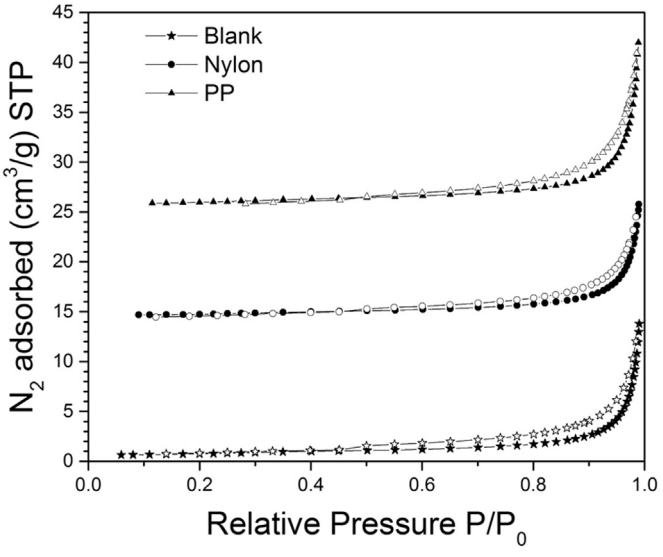

Fig. 10. N_2 adsorption/desorption isotherms of blank, nylon- and PP- based samples (maximum fibers loading); the data were stacked on y-axis for the sake of clarity. Fill and open symbols represent adsorption and desorption branches, respectively.

4. Conclusions

Nylon 6,6 and polypropylene fibers were successfully employed as pore-forming agents in LaC_x disks synthesized from La_2O_3 and graphite powders. Additions up to 21.3 vol% of nylon or up to 24.8 vol% of PP fibers were employed to enhance the pore interconnectivity and the permeability of bodies. Due to the processing method, fibers were oriented along the plane perpendicular to the loading direction, with creation of a network of interconnected pores in the radial direction after sintering. Despite the univocal and linear increase in total porosity ($\approx 25\%$), the resulting increase of permeability coefficients achieved two orders of magnitude for k_1 and three orders for k_2 in relation to the blank sample. Compared under similar volumetric contents, nylon 6,6 was slightly more effective than polypropylene to enhance permeability. The effect was ascribed to the superior mechanical properties of nylon, which possibly yielded smoother and more interconnected pores. Compared to spherical pore formers (PMMA beads), polymeric fibers were much more effective to enhance the permeability of porous LaC_x targets for the SPES project.

Acknowledgments

Authors would like to thank D. Mella and M. Lollo of INFN-LNL for their precious scientific and technological support. M.D.M. Innocentini also thanks R.F. Caldato of UNAERP for the laboratory work and CNPq (Project 303962/2015-1)- Brazil for the financial support.

References

[1] B. Hy, N. Barré-Boscher, A. Ozgumus, B. Roussiere, S. Tusseau-Nenez, C. Lau, M. Cheikh Mhamed, M. Raynaud, A. Said, K. Kolos, E. Cottereau, S. Essabaa, O. Tougait, M. Pasturel, An off-line method to characterize the fission product release from uranium carbide-target prototypes developed for SPIRAL2 project, Nucl. Instrum. Methods Phys. Res. B 288 (2012) 34–41.
[2] L. Biasetto, S. Carturan, G. Maggioni, P. Zanonato, P. Di Bernardo, P. Colombo, A. Andrighetto, G. Prete, Fabrication of mesoporous and high specific surface area lanthanum carbide–carbon nanotube composites, J. Nucl. Mater. 385 (2009) 582–590.
[3] L. Biasetto, P. Zanonato, S. Carturan, P. Di Bernardo, P. Colombo, A. Andrighetto, G. Prete, Lanthanum carbide-based porous materials from carburization of lanthanum oxide and lanthanum oxalate mixtures, J. Nucl. Mater. 378 (2008) 180–187.
[4] S. Corradetti, L. Biasetto, M. Manzolaro, D. Scarpa, S. Carturan, A. Andrighetto, G. Prete, J. Vasquez, P. Zanonato, P. Colombo, C.U. Jost, D.W. Stracener, Neutron-rich isotope production using a uranium carbide – carbon nanotubes SPES target prototype, Eur. Phys. J. A 49 (2013) 56–65.
[5] J.P. Ramos, C.M. Fernandes, T. Stora, A.M.R. Senos, Sintering kinetics of nanometric calcium oxide in vacuum atmosphere, Ceram. Int. 41 (2015) 8093–8099.
[6] G.J. Dienes, A.C. Damask, Radiation enhanced diffusion in solids, J. Appl. Phys. 29 (1958) 1713–1721.
[7] R. Kirchner, On the release and ionization efficiency of catcher-ion-source systems in isotope separation on-line, Nucl. Instrum. Methods Phys. Res. B 70 (1992) 186–199.
[8] A. Monetti, A. Andrighetto, C. Petrovich, M. Manzolaro, S. Corradetti, D. Scarpa, F. Rossetto, F. Martinez Dominguez, J. Vasquez, M. Rossignoli, M. Calderolla, R. Silingardi, A. Mozzi, F. Borgna, G. Vivian, E. Boratto, M. Ballan, G. Prete, G. Meneghetti, The RIB production target for the SPES project, Eur. Phys. J. A 51 (2015) 128–138.
[9] L. Biasetto, M.D.M. Innocentini, W.S. Chacon, S. Corradetti, S. Carturan, P. Colombo, A. Andrighetto, Gas permeability of lanthanum oxycarbide targets for the SPES project, J. Nucl. Mater. 440 (2013) 70–80.
[10] K. Okada, M. Shimizu, T. Isobe, Y. Kameshima, M. Sakai, A. Nakajima, T. Kurata, Characteristics of microbubbles generated by porous mullite ceramics prepared by an extrusion method using organic fibers as the pore former, J. Eur. Ceram. Soc. 30 (2010) 1245–1251.
[11] H.R. Rasouli, F. Golestani-Fard, A.R. Mirhabibi, G.M. Nasab, K.J.D. Mackenzie, M. H. Shahraki, Fabrication and properties of microporous metakaolin-based geopolymer bodies with polylactic acid (PLA) fibers as pore generators, Ceram. Int. 41 (2015) 7872–7880.
[12] M.D.M. Innocentini, R. Salomão, C. Ribeiro, F.A. Cardoso, L.R.M. Bittencourt, R. P. Rettore, V.C. Pandolfelli, Permeability of fiber-containing refractory castables

– Part 1, Am. Ceram. Soc. Bull. 81 (2002) 34–37.
[13] M.D.M. Innocentini, R. Salomão, C. Ribeiro, F.A. Cardoso, L.R.M. Bittencourt, R. P. Rettore, V.C. Pandolfelli, Permeability of fiber-containing refractory castables – Part 2, Am. Ceram. Soc. Bull. 81 (2002) 65–68.
[14] L. Mandecka-Kamień, A. Rapacz-Kmitan, Ł. Wójcik, The effect of the addition of polypropylene fibres on the properties of corundum refractory concretes with a low cement content and an addition of aluminium phosphate, Ceram. Int. 40 (2014) 15663–15668.
[15] R. Salomão, F.A. Cardoso, M.D.M. Innocentini, L.R.M. Bittencourt, V. C. Pandolfelli, Effect of polymeric fibers on refractory castables permeability, Am. Ceram. Soc. Bull. 82 (2003) 51–56.
[16] R. Salomão, C.S. Isaac, F.A. Cardoso, M.D.M. Innocentini, V.C. Pandolfelli, PSD, polymeric fibers and the permeability of refractory castables, Am. Ceram. Soc. Bull. 82 (2003) 931–935.
[17] M.D.M. Innocentini, R. Salomão, C. Ribeiro, L.R.M. Bittencourt, V.C. Pandolfelli, Assessment of mass loss and permeability changes during the dewatering process of refractory castables containing polypropylene fibers, J. Am. Ceram. Soc. 85 (2002) 2110–2112.
[18] M.D.M. Innocentini, W.S. Chacon, R.F. Caldato, G.P. Rocha, G.L. Adabo, Microstructural, physical, and fluid dynamic assessment of spinel-based and phosphate-bonded investments for dental applications, Int. J. Appl. Ceram. Technol. 52 (2013) 18362–18372.
[19] S. Corradetti, S. Carturan, L. Biasetto, A. Andrighetto, P. Colombo, Boron carbide as a target for the SPES project, J. Nucl. Mater. 432 (2013) 212–221.
[20] S. Corradetti, A. Andrighetto, M. Manzolaro, D. Scarpa, J. Vasquez, M. Rossignoli, A. Monetti, M. Calderolla, G. Prete, Research and development on materials for the SPES target, Eur. Phys. J. Web Conf. 66 (2014) 1–4.
[21] K.S.W. Sing, D.H. Everett, R.A.W. Haul, L. Moscou, R.A. Pierotti, J. Rouquerol, T. Siemieniewska, Reporting physisorption data for gas/solid systems with special reference to the determination of surface area and porosity, Pure Appl. Chem. 57 (1985) 603–619.
[22] S. Brunauer, P.H. Emmett, E. Teller, Adsorption of gases in multimolecular layers, J. Am. Chem. Soc. 60 (1938) 309–319.
[23] M.D.M. Innocentini, P. Sepulveda, F. Ortega, Permeability, in: M. Scheffler, P. Colombo (Eds.), Cellular Ceramics: Structure, Manufacturing, Properties and Applications, Wiley-VCH, Weinheim, Germany, 2005, pp. 313–341.
[24] J.D. Peterson, S. Vyazovkin, C.A. Wight, Kinetics of the thermal and thermo-oxidative degradation of polystyrene, polyethylene and poly(propylene), Macromol. Chem. Phys. 202 (2001) 775–784.
[25] S. Ray, R.P. Cooney, Thermal degradation of polymer and polymer composites, in: M. Kutz (Ed.), Handbook of Environmental Degradation of Materials, 2nd ed.,William Andrew, Waltham (MA), USA, 2012, pp. 213–242.
[26] L. Biasetto, P. Zanonato, S. Carturan, P. Di Bernardo, P. Colombo, A. Andrighetto, G. Prete, Developing uranium dicarbide–graphite porous materials for the SPES project, J. Nucl. Mater. 404 (2010) 68–76.
[27] T. Isobe, Y. Kameshima, A. Nakajima, K. Okada, Y. Hotta, Gas permeability and mechanical properties of porous alumina ceramics with unidirectionally aligned pores, J. Eur. Ceram. Soc. 27 (2007) 53–59.
[28] T. Isobe, T. Tomita, Y. Kameshima, A. Nakajima, K. Okada, Preparation and properties of porous alumina ceramics with oriented cylindrical pores produced by an extrusion method, J. Eur. Ceram. Soc. 26 (2006) 957–960.
[29] K. Okada, S. Uchiyama, T. Isobe, Y. Kameshima, A. Nakajima, T. Kurata, Capillary rise properties of porous mullite ceramics prepared by an extrusion method using organic fibers as the pore former, J. Eur. Ceram. Soc. 29 (2009) 2491–2497.
[30] K. Okada, A. Imase, T. Isobe, A. Nakajima, Capillary rise properties of porous geopolymers prepared by an extrusion method using polylactic acid (PLA) fibers as the pore formers, J. Eur. Ceram. Soc. 31 (2011) 461–467.
[31] C. Yuan, S. Jones, Investigation of fibre modified ceramic moulds for investment casting, J. Eur. Ceram. Soc. 23 (2003) 399–407.
[32] R. Salomão, V.C. Pandolfelli, The particle size distribution effect on the drying efficiency of polymeric fibers containing castables, Ceram. Int. 34 (2008) 173–180.
[33] R. Salomão, A.M. Zambon, V.C. Pandolfelli, Polymeric fiber geometry affects refractory castable permeability, Am. Ceram. Soc. Bull. 85 (2006) 9201–9205.
[34] B. Collignon, C. Moyne, J.-L. Guichard, C. Perrot, Y. Jannot, Modelling the pressure dependence and the influence of added polymeric fibers on the permeability of refractory concretes, Ceram. Int. 37 (2011) 627–634.
[35] P.S. Song, S. Hwang, B.C. Sheu, Strength properties of nylon- and polypropylene-fiber-reinforced concretes, Cem. Concr. Res. 35 (2005) 1546–1550.
[36] L. Biasetto, P. Colombo, M.D.M. Innocentini, S. Mullens, Gas permeability of microcellular ceramic foams, Ind. Eng. Chem. Res. 46 (2007) 3366–3372.
[37] M.D.M. Innocentini, R.G. Pileggi, F.T. Ramal Jr., V.C. Pandolfelli, Permeability and drying behavior of PSD-designed refractory castables, Am. Ceram. Soc. Bull. 82 (7) (2003) 1–6.
[38] S. Tusseau-Nenez, B. Roussière, N. Barré-Boscher, A. Gottberg, S. Corradetti, A. Andrighetto, M. Cheikh Mhamed, S. Essabaa, H. Franberg-Delahaye, J. Grinyer, L. Joanny, C. Lau, J. Le Lannic, M. Raynaud, A. Saïd, T. Stora, O. Tougait, Characterization of uranium carbide target materials to produce neutron-rich radioactive beams, Nucl. Instrum. Methods Phys. Res. B 370 (2016) 19.
[39] F.J. O'Brien, B.A. Harley, M.A. Waller, I.V. Yannas, L.J. Gibson, The effect of pore size on permeability and cell attachment in collagen scaffolds for tissue engineering, Technol. Health Care 15 (2007) 3–17.